The Astrophysical Journal, 775:65 (7pp), 2013 September 20 doi:10.1088/0004-637X/775/1/65

NuSTAR DETECTION OF HARD X-RAY PHASE LAGS FROM THE ACCRETING PULSAR GS 0834−430

Hiromasa Miyasaka[1], Matteo Bachetti[2,3], Fiona A. Harrison[1], Felix Fürst[1], Didier Barret[2,3], Eric C. Bellm[1], Steven E. Boggs[4], Deepto Chakrabarty[5], Jerome Chenevez[6], Finn E. Christensen[6], William W. Craig[4,7], Brian W. Grefenstette[1], Charles J. Hailey[8], Kristin K. Madsen[1], Lorenzo Natalucci[9], Katja Pottschmidt[10], Daniel Stern[11], John A. Tomsick[4], Dominic J. Walton[1], Jörn Wilms[12], and William Zhang[13]
[1] Cahill Center for Astronomy and Astrophysics, California Institute of Technology, Pasadena, CA 91125, USA; miyasaka@srl.caltech.edu
[2] Université de Toulouse, UPS-OMP, IRAP, F-31400 Toulouse, France
[3] CNRS, Institut de Recherche en Astrophysique et Planétologie, 9 Av. colonel Roche, BP 44346, F-31028 Toulouse cedex 4, France
[4] Space Sciences Laboratory, University of California, Berkeley, CA 94720, USA
[5] Kavli Institute for Astrophysics and Space Research, Massachusetts Institute of Technology, Cambridge, MA 02139, USA
[6] DTU Space, National Space Institute, Technical University of Denmark, Elektrovej 327, DK-2800 Lyngby, Denmark
[7] Lawrence Livermore National Laboratory, Livermore, CA 94550, USA
[8] Columbia Astrophysics Laboratory, Columbia University, New York, NY 10027, USA
[9] Istituto di Astrofisica e Planetologia Spaziali, INAF, Via Fosso del Cavaliere 100, Roma I-00133, Italy
[10] CRESST, UMBC, and NASA GSFC, Code 661, Greenbelt, MD 20771, USA
[11] Jet Propulsion Laboratory, California Institute of Technology, Pasadena, CA 91109, USA
[12] Dr. Karl-Remeis-Sternwarte and ECAP, Sternwartstr. 7, D-96049 Bamberg, Germany
[13] NASA Goddard Space Flight Center, Greenbelt, MD 20771, USA
Received 2013 June 3; accepted 2013 July 25; published 2013 September 5

ABSTRACT

The *Nuclear Spectroscopic Telescope Array* hard X-ray telescope observed the transient Be/X-ray binary GS 0834−430 during its 2012 outburst—the first active state of this system observed in the past 19 yr. We performed timing and spectral analysis and measured the X-ray spectrum between 3–79 keV with high statistical significance. We find the phase-averaged spectrum to be consistent with that observed in many other magnetized, accreting pulsars. We fail to detect cyclotron resonance scattering features that would allow us to constrain the pulsar's magnetic field in either phase-averaged or phase-resolved spectra. Timing analysis shows a clearly detected pulse period of ∼12.29 s in all energy bands. The pulse profiles show a strong, energy-dependent hard phase lag of up to 0.3 cycles in phase, or about 4 s. Such dramatic energy-dependent lags in the pulse profile have never before been reported in high-mass X-ray binary pulsars. Previously reported lags have been significantly smaller in phase and restricted to low energies ($E < 10$ keV). We investigate the possible mechanisms that might produce this energy-dependent pulse phase shift. We find the most likely explanation for this effect is a complex beam geometry.

Key words: binaries: general – pulsars: individual (GS 0834-430) – stars: neutron – X-rays: binaries

Online-only material: color figures

1. INTRODUCTION

The transient X-ray source GS 0834−430 was discovered in outburst by the *Granat*/WATCH X-ray sky monitor in 1990 (Sunyaev 1990; the source was named GRS 0831−429). Subsequent observations by *Ginga* (Aoki et al. 1992), *ROSAT* (Belloni et al. 1993), and *Granat*/ART-P (Sunyaev 1991) identified a 12.3 s period pulsar with a low (∼10%) pulsed fraction. The BATSE all-sky monitor on the *Compton Gamma-Ray Observatory* detected seven outbursts from GS 0834−430 over the period 1991 April–1993 June (Wilson et al. 1997). The first five outbursts occurred at a regular spacing of about 106 days, while the last two outbursts were spaced by about 140 days. Using the first five BATSE-detected outbursts, Wilson et al. (1997) determined 1σ limits on the orbital period of $P_{\rm orb} = 105.8 \pm 0.4$ days and on the eccentricity of $0.10 < e < 0.17$. Subsequently, the source became dormant for a period of 19 yr.

The hard spectrum, the recurring nature of the outbursts, and the presence of pulsations suggest that GS 0834−430 is a Be/X-ray binary with a magnetized neutron star accreting from the dense equatorial wind of its companion (Belloni et al. 1993). A low orbital inclination could explain the low pulsed fraction, assuming that the spin and orbital angular momentum vectors are aligned (Wilson et al. 1997). The low orbital eccentricity and the combination of regular and irregular outbursts of similar intensity are unusual for such systems. Israel et al. (2000) identified the optical counterpart, most likely a B0–2 V–IIIe spectral type star located at a distance of ∼5 kpc, confirming the Be-star/X-ray binary nature of GS 0834−430.

The initial observations noted unusual features in the pulse profile as a function of energy. Both Aoki et al. (1992) and Wilson et al. (1997) reported a variation of the pulse shape with energy, with a primary and a secondary peak dominant in different energy bands. Wilson et al. (1997) remarked on the presence of some shifts between profiles in different energy bands, but did not discuss this result further. Significant phase shifts as a function of energy in accreting pulsars are rare; this observation of phase shifts singles out GS 0834−430 as an interesting object for phase-resolved spectroscopy.

On UT 2012 June 26, *INTEGRAL* (Winkler et al. 2003), during one of its Galactic plane scans, discovered that GS 0834−430 was in outburst for the first time in 19 yr, with a 18–60 keV flux of 109 mCrab (Drave et al. 2012). *Swift* (Burrows et al. 2005) measured an absorption column of $2.2^{+2.63}_{-1.66} \times 10^{22}$ cm^{-2} (Barthelmy et al. 2012) and *Fermi*/Gamma-ray Burst Monitor (GBM; Meegan et al. 2009) detected pulsations with a barycentric frequency of 81.3357(4) mHz on

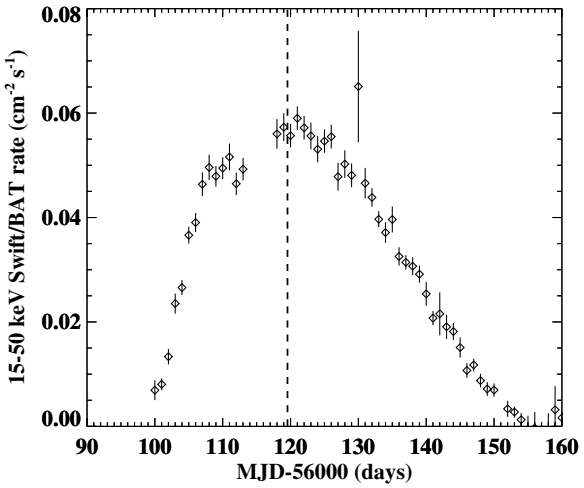

Figure 1. *Swift*/BAT light curve in the 15–50 keV range for GS 0834−430 during the 2012 July outburst. The vertical dashed line marks the midpoint of the *NuSTAR* observation, which occurred at the very peak of the outburst.

UT June 28–30 and 81.3377(3) mHz on UT June 30–July 2[14] (Jenke et al. 2012).

On UT July 11, at the peak of the outburst (see Figure 1), the *Nuclear Spectroscopic Telescope Array* (*NuSTAR*; Harrison et al. 2013) observed GS 0834−430 for about 30 ks. In this paper, we present these data, including the first phase-resolved spectroscopy simultaneously spanning the entire energy range from 3–79 keV.

2. OBSERVATIONS AND DATA REDUCTION

NuSTAR is the first focusing high-energy X-ray telescope in space, sensitive between 3–79 keV. Two grazing incidence optics focus X-rays onto two independent Cadmium Zinc Telluride (CZT) detectors called Focal Plane Modules A and B (FPMA and FPMB, respectively). For a detailed description of the instrument, see Harrison et al. (2013).

NuSTAR observed GS 0834−430 on 2012 July 11 from 02:40:00–23:40:00 UT as part of its observatory commissioning program. The total exposure time, corrected for dead time, Earth occultation, and South Atlantic Anomaly (SAA) passages, was 31.0 ks. The total dead time-corrected count rate was 52.01 ± 0.05 counts s^{-1} (3–79 keV) in each of the two coaligned telescope modules. For these observations, the source was placed near the optical axis on detector 0 (see Harrison et al. 2013 for details of the focal plane layout). Individual photons are time-tagged to a relative accuracy of 2 μs and the absolute (relative to UT) calibration of the onboard clock is good to 2 ms rms. The spectral resolution ranges from 400 eV (FHWM) at 10 keV to 1 keV (FWHM) at 79 keV.

We reduced and analyzed the data using the *NuSTAR Data Analysis Software* v1.1.1 and CALDB version 20130509. The data were filtered for intervals of high background due to SAA passages. To extract data for spectral analysis, we used a circular aperture of radius 65″ centered on the source position. We determined the background by extracting counts from a region 100″ in radius on a different detector than the source, since GS 0834−430 is bright and the point spread function (PSF) wings contaminate most of detector 0. At 10 keV, the source is 10^3 times brighter than the background and at 80 keV the source is still 10 times above the background, so small systematics uncertainties due to choosing a different chip for background subtraction are unimportant. We rebinned the spectrum in order to have at least 50 counts channel^{-1}.

[14] See the full period evolution, as detected by GBM, at http://gammaray.nsstc.nasa.gov/gbm/science/pulsars/lightcurves/gs0834.html.

Table 1
Ephemeris for GS0834−430 (Wilson et al. 1997)

Projected semi-major axis	$a_x \sin i$ (lt-s)	128^{+47}_{-38}
Orbital period at the epoch	$P_{\rm orb}$ (days)	105.8 ± 0.4
Eccentricity × $a_x \sin i$	$e\, a_x \sin i$ (lt-s)	$15.3^{+3.3}_{-0.9}$
Longitude of periastron	ω (deg)	140^{+35}_{-53}
Epoch for mean longitude of 90°	T_{90} (MJD)	48809.5

3. PULSE PROFILE ANALYSIS

3.1. Pulse Period Determination

In order to determine the pulse period of GS 0834−430, we first corrected the photon arrival times to the solar system barycenter using the HEASARC FTOOL `barycorr`, with the default DE−200 solar system ephemeris, adopting the sky position measured by *ROSAT* (Belloni et al. 1993; $\alpha = 8^{\rm h}35^{\rm m}55\overset{\rm s}{.}1$, $\delta = -43^\circ 11' 22''$, J2000) and the orbital ephemeris determined by Wilson et al. (1997), which is given in Table 1. We determined the pulse period of GS 0834−430 using an epoch folding technique (Leahy et al. 1983). A Z^2_3 analysis (Buccheri et al. 1983) yields a period of 12.293(1) s. This period is consistent with the range measured by GBM. We note that the period is not stable due to the combination of spin-down and spin-up due to accretion torque (Davidson & Ostriker 1973), but does not change significantly over the *NuSTAR* observations. We measure a pulsed fraction, defined as the ratio of the half amplitude of the pulse to the mean count rate, of 15.5(4)% over the whole energy range, going up to 18.3(8)% in the 40–80 keV range. These values are comparable to the BATSE measurement (Wilson et al. 1997) of $\lesssim$15% in the 20–50 keV range. Figure 12 from that work also shows best-fit values of ∼15%–40% in the 50–70 keV band for several BATSE observations, providing marginal evidence for an increase in the pulse fraction with energy.

3.2. Energy-dependent Pulse Profile

Figure 2 shows the pulse profile in five different energy bands over phase range 0 to 2 (two pulse cycles). Phase 0 is chosen to be at MJD 56119.203555. The pulse profile is clearly stable and strongly dependent on energy. Two peaks are visible, a secondary (smaller) peak in the 3–6 keV band at phase ∼0.2 and a larger peak at phase ∼0.8. It is also clear that the phase of the larger peak shifts significantly with increasing X-ray energy, such that in the 20–40 keV band it has shifted in phase by 0.3 cycles (peaking at phase 0.1). Such a large and dramatic energy dependence has not been previously observed in any accreting X-ray pulsar. In the 40–80 keV range, the secondary peak becomes dominant (peaking at phase ∼1.4).

Figure 3 shows a map of the DC level-subtracted pulse profile as a function of energy. The binning is variable over the map, in order to attain a better signal-to-noise ratio (S/N), as explained in the figure caption. Focusing on the strongest feature that peaks at phase 0.8 in the softest bands, there is a clear and almost linear shift of the pulse peak with energy until phase ∼1.1. To better investigate the behavior of the profile with energy, we fit every average profile with a double Gaussian. The result of this

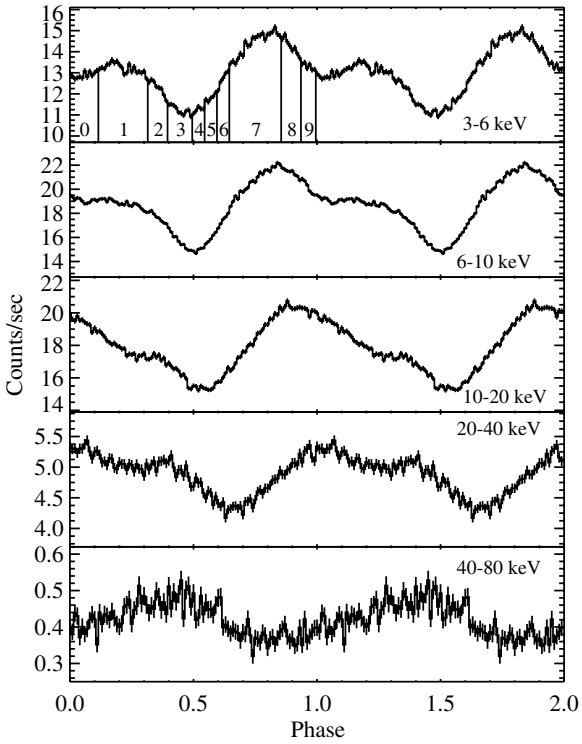

Figure 2. Pulse profile in four different energy bands. A strong dependence with energy is clearly visible. Intervals in the top pulse profile show the phases used for phase-resolved spectroscopy (see Section 5).

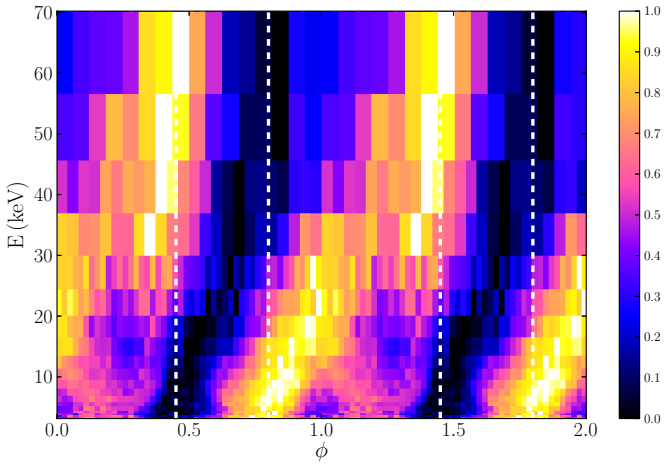

Figure 3. Evolution of the DC level-subtracted pulse profile with energy. We started from a map where every profile was calculated in an energy band of ∼0.4 keV and was divided into 48 bins. In order to attain a better S/N at high energy, we then averaged over an increasing number of bins at higher energies, following approximately a geometrical progression both in phase and in energy. Each profile is background subtracted and normalized from 0 to 1. This normalized rate is color coded, ranging from the lowest count rates in black to the highest count rates in white. The profiles are repeated twice in phase for clarity. The white dashed lines indicate roughly the phase of the peak and the dip, respectively, at the softest energies, to guide the eye. The image is not smoothed and the noise at high energy is due to the poor statistics. The minimum and the peak of the profiles are shifting in phase with energy, showing a clear hard lag.

(A color version of this figure is available in the online journal.)

procedure is shown in Figure 4. The two peaks move in phase in a quasi-parallel fashion below ∼30 keV, where the first peak is dominant over the second. Around 35 keV, the secondary peak becomes dominant. At higher energies, the primary peak

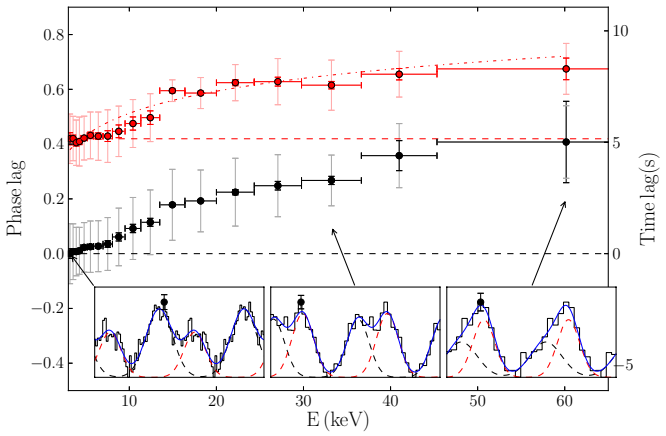

Figure 4. Phase lags of the two peaks, obtained by fitting each rebinned profile in Figure 3 with two independent Gaussians, relative to the phase of the first peak in the lowest energy band. The black corresponds to the main peak and the red corresponds to the secondary peak. The full-color error bars are 1σ uncertainties. The light-colored error bars indicate the HWHM of the Gaussians. The dashed lines show the phase of the two peaks in the lowest energy band. The dash-dotted line indicates the best fit of Equation (4) to the secondary peak lags (see also Section 6). We chose the secondary peak because it is better constrained over the whole energy range. The insets show the fit in the first energy band, at ∼35 keV where the secondary peak becomes dominant, and in the last energy band, respectively.

(A color version of this figure is available in the online journal.)

becomes wider and less significant and the behavior is less clear. The only evidence for the presence of the primary peak is the fact that the high-energy profile has different slopes on the two sides, providing a hint of a small contribution from the fading primary peak.

4. PHASE-AVERAGED SPECTRUM

The phase-averaged X-ray spectrum of GS 0834−430 is broadly similar to that seen in many X-ray binary pulsars, with gradual curvature and a high-energy cutoff. A weak narrow iron feature is also evident in the spectrum (Figure 5).

A number of largely empirical models have been developed to describe the broad-band X-ray spectra of accreting pulsars (see Müller et al. 2013 for a summary of pulsar continuum models). In the following, we will apply some of the most common models to our spectrum using the XSPEC software (Arnaud 1996). The column density is not constrained by the *NuSTAR* data alone and since the low-energy residuals indicate no excess absorption and past observations did not indicate column densities substantially different from the Galactic value, we fixed the column density to the Galactic value 1.010×10^{22} cm^{-2} (Kalberla et al. 2005) in all spectral fits (through the `tbabs` model; Wilms et al. 2000).

We first attempted to fit the 3–79 keV spectrum with a Gaussian iron line plus an absorbed, cutoff power law, where the continuum model has the following form:

$$\mathrm{CutoffPL}(E) \propto E^{-\Gamma} \exp\left(-E/E_{\mathrm{fold}}\right). \quad (1)$$

This model fails to adequately describe the spectrum, with a best-fit χ^2 of 6864 for 2068 degrees of freedom. We tried to add a Gaussian line around 10 keV to improve the fit. This "10 keV feature" is seen in many accreting neutron stars, however, its physical origin is unclear (Coburn et al. 2002; Müller et al. 2013). The quality of the fit clearly improved to a χ^2 of 2482 for 2066 degrees of freedom when fixing the energy of the

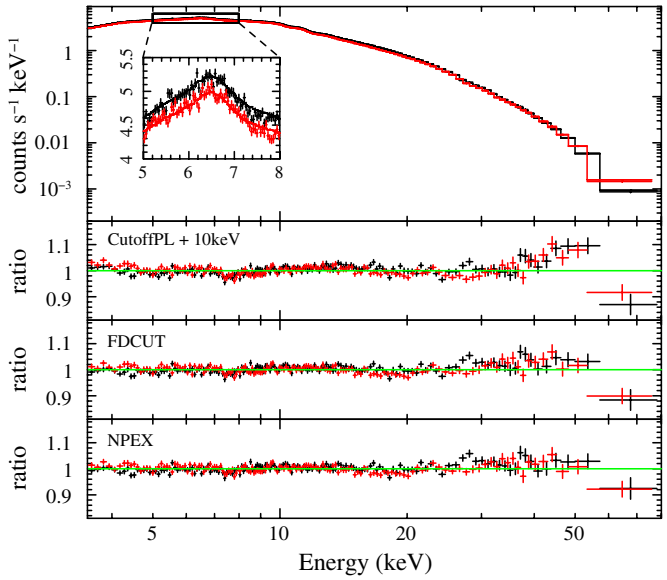

Figure 5. Phase-averaged spectrum fit using the NPEX continuum model. Black points represent data from FPMA and the red points correspond to data from FPMB. The top panel shows the counts spectrum, with the data-to-model ratio for CutoffPL+10 keV, FDCUT, and NPEX shown in the second, third, and fourth panels, respectively. The region around the iron line is shown in the inset.

(A color version of this figure is available in the online journal.)

Table 2
Fit Parameters for the FDCUT Model

$N_{\rm H}$	=	1.010×10^{22} cm^{-2} (fixed)
Γ	=	0.64 ± 0.01
A	=	$(9.04 \pm 0.06) \times 10^{-2}$ photons keV^{-1} cm^{-2} s^{-1}
$E_{\rm cutoff}$	=	18.19 ± 0.37 keV
$E_{\rm fold}$	=	10.10 ± 0.07 keV
$E_{\rm Fe}$	=	6.51 ± 0.03 keV
$\sigma_{\rm Fe}$	=	0.27 ± 0.04 keV
$A_{\rm Fe}$	=	$(1.06 \pm 0.10) \times 10^{-3}$ photons cm^{-2} s^{-1}

Notes. All uncertainties refer to single-parameter 90% confidence limits. The χ^2 is 2319 for 2067 degrees of freedom. Parameter names are defined in Equation (2).

feature to exactly 10 keV (see residuals in Figure 5). However, the best width was around 14 keV, clearly broader than typically expected for this feature. Leaving the centroid energy free did not result in an improvement in the fit. We therefore rule out a model of a simple cutoff power law plus a 10 keV feature.

In order to obtain an adequate spectral fit, we need models with a more flexible continuum shape. We found adequate fits using both the Negative and Positive power-law Exponential (NPEX; Mihara 1995; Makishima et al. 1999) and the "Fermi Dirac Cutoff" (FDCUT; Tanaka 1986) models. Using the FDCUT model, the continuum is characterized by

$$\mathrm{FDCUT}(E) \propto A \times E^{-\Gamma} \frac{1}{1+\exp\left((E-E_{\rm cutoff})/E_{\rm fold}\right)}. \quad (2)$$

Additionally, we applied a Galactic absorption column $N_{\rm H}$ and a Gaussian iron line to describe the Fe Kα line (with energy $E_{\rm Fe}$, width $\sigma_{\rm Fe}$, and normalization $A_{\rm Fe}$). The model is defined in XSPEC as `const*tbabs*(power*fdcut+gauss)`. We obtain a best-fit $\chi^2 = 2266$ for 2067 degrees of freedom. Figure 5 shows the fit residuals and Table 2 lists the best-fit parameters with errors. The residuals clearly indicate that the sharpness of the spectral curvature is not perfectly captured above 30 keV.

Table 3
Fit Parameters for the NPEX Model

$N_{\rm H}$	=	1.010×10^{22} cm^{-2} (fixed)
α	=	0.38 ± 0.05
β	=	1.50 ± 0.09
kT	=	7.30 ± 0.14 keV
A_n	=	$(7.75^{+0.35}_{-0.31}) \times 10^{-2}$ photons keV^{-1} cm^{-2} s^{-1}
A_p	=	$(7.76^{+1.87}_{-1.48}) \times 10^{-4}$ photons keV^{-1} cm^{-2} s^{-1}
$E_{\rm Fe}$	=	6.51 ± 0.03 keV
$\sigma_{\rm Fe}$	=	0.27 ± 0.04 keV
$A_{\rm Fe}$	=	$(1.07 \pm 0.11) \times 10^{-3}$ photons cm^{-2} s^{-1}

Notes. All uncertainties refer to single-parameter 90% confidence limits. The χ^2 is 2234 for 2066 degrees of freedom. Parameter names are defined in Equation (3).

Using the NPEX model, with a continuum characterized by

$$\mathrm{NPEX}(E) \propto (A_n E^{-\alpha} + A_p E^{+\beta}) \exp(-E/kT), \quad (3)$$

we obtain a somewhat better characterization. The negative and positive power-law components have independent normalizations A_n and A_p, respectively, but are multiplied by the same exponential turn-over, characterized by the temperature kT. Figure 5 shows the best-fit residuals and Table 3 provides the best-fit parameters. The best-fit $\chi^2 = 2234$ for 2066 degrees of freedom. While neither of these models provides a formally acceptable fit, the characterization is adequate to understand the basic continuum and compare the spectral shape with other accreting pulsar systems.

From the best-fit, phase-averaged spectrum using the NPEX model, we find the flux to be $(6.659 \pm 0.001) \times 10^{-9}$ erg s^{-1} cm^{-2} (3.5–80 keV). Wilson et al. (1997) use measurements of the pulsar spin-up during outburst to place a lower limit on the distance to GS 0834−430 of $d \geqslant 4.5$ kpc. Israel et al. (2000) place a higher limit on the distance of 6 kpc based on considerations on the spectral type of the companion star and the extinction of the source. Adopting a distance of 5 kpc implies a 3.5–80 keV unabsorbed luminosity of $(2.002 \pm 0.002) \times 10^{37}$ erg s^{-1}.

5. PHASE-RESOLVED SPECTRAL ANALYSIS

To further characterize the phase dependence of the spectrum, we decomposed the pulse profile into 10 phase bins chosen to finely sample ranges where the hardness ratio (HR) is changing rapidly; we define the HR as the ratio of the difference and the sum of the 20–40 and 4–7 keV fluxes. We then fit the phase intervals using the NPEX model described above in order to determine the dependence of the model parameters on phase. The positive power-law term is fixed to $\beta = 1.50$, which is obtained from the phase-averaged spectrum due to the better statistical constraints. We found that this value of β describes all 10 phase bins between 3.5–65 keV very well, with reduced χ^2 values between 0.97–1.06. Figure 6 (top panel) shows the HR as a function of phase. The HR is at a minimum at phase 0.7, roughly coincident with the primary maximum in the soft 3–6 keV profile, and has a maximum 0.85 later in phase, similar to that seen in the raw counts as a function of phase. The lower four panels in Figure 6 show the strong dependence of spectral fit parameters on pulse phase. The two peaks in the HR, between phases 0.4–0.65 and 0.8–1.1, originate from different changes in the spectra. The first peak, coincident with the minimum in the soft pulse profiles, has a higher value of α. That means that the

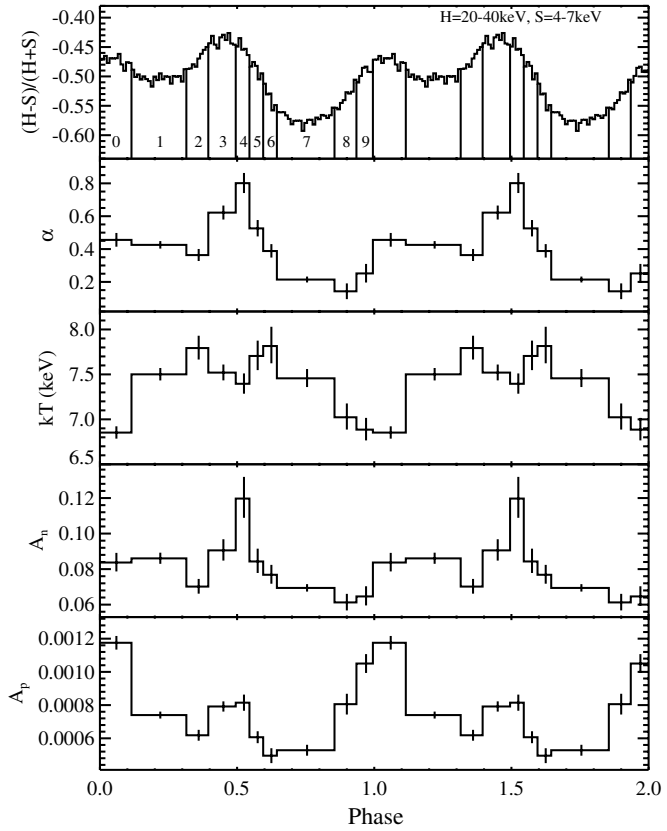

Figure 6. Hardness ratio between the 20–40 keV and 4–7 keV bands as a function of pulse phase (top panel). Intervals have been chosen based on the evolution of the hardness ratio to fit NPEX model parameters. The lower four panels show the evolution of fit parameters as a function of pulse phase, i.e., the photon index of the negative power law (α), the cutoff energy kT, the normalization of the negative power-law component A_n, and the normalization of the positive power-law component A_p. The positive power-law term is fixed to $\beta = 1.50$. The pulse is repeated once for clarity. The error bars are the same as in Table 3.

soft component, described by α and A_n, falls off more quickly, resulting in an overall harder spectrum. The second peak in the HR, on the other hand, occurs during the broad peak of the 20–40 keV pulse profile. Here, the change in hardness is mainly due to a drastically increased normalization of the positive power-law component A_p, which dominates the spectrum above ~20 keV.

Cyclotron resonance scattering features (CRSFs) are observed in some accreting X-ray pulsars between 5–100 keV (see Coburn et al. 2006 for a review) and yield the only direct measurements of the neutron star magnetic field through the Landau relation $E_{\rm cyc} = \hbar eB/m_e c = 11.6\,{\rm keV}\,B_{12}$, where B_{12} is the magnetic field in units of 10^{12} G. In order to search for CRSFs that might provide such measurements, we examined the fit residuals in the phase-resolved, as well as the phase-averaged, spectra. It has been shown that the exact parameters of a CRSF depend on the chosen continuum (see, e.g., Müller et al. 2013). The NPEX continuum in particular has been found to change the parameters to unphysical values. However, the NPEX model applied here is smooth in the relevant range for the line (>20 keV), so a CRSF would show up as a deviation in the continuum. After a careful examination of the residuals, we see no systematic features that would indicate the presence of a CRSF in this source.

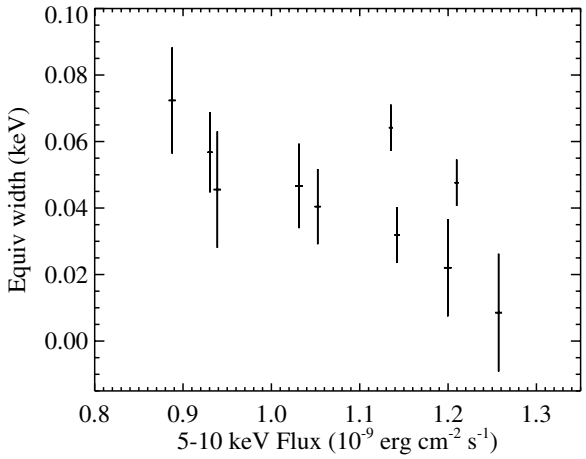

Figure 7. Scatter plot of iron line equivalent width vs. 5–10 keV X-ray flux.

This negative result of our search could be because the magnetic field of the source is such that possible cyclotron lines are outside of *NuSTAR*'s bandwidth. This fact would, however, imply a magnetic field $B \geqslant 5\times10^{12}$ G, higher than any confirmed field in a high-mass X-ray binary (HMXB; Caballero & Wilms 2012). On the other hand, the line is possible that the fundamental cyclotron line gets filled up with spawned photons from higher harmonics, making the line undetectable in the X-ray spectrum (Schönherr et al. 2007). This scenario has also been discussed for 4U 1909+07, another pulsating HMXB without a detectable CRSF (Fürst et al. 2012). We therefore cannot draw direct conclusions about the magnetic field strength of GS 0834−430.

5.1. Evolution of the Iron Line

Fe Kα lines are ubiquitous in spectra of Be/X-ray binaries and while their equivalent widths do not change significantly with luminosity, their fluxes are generally proportional to the total flux of the source (see, e.g., Reig & Nespoli 2013). In these systems, Fe Kα lines are usually consistent with being produced by fluorescence in a cold, quasi-neutral material probably belonging to the circumstellar material. We fit a Gaussian line to every phase of the pulse in order to study the pulse evolution. Figure 7 shows the equivalent width of the Fe Kα line, obtained by fitting a Gaussian line with an underlying NPEX continuum model, as a function of soft flux. We observe no significant variation in the line energy, while it appears that the line equivalent width is mildly anticorrelated with the 5–10 keV flux. Such a behavior is expected if the line emission is constant with pulse phase and is being diluted by an increased continuum level. This result argues in favor of the line produced far from the accretion column, consistent with the general behavior mentioned above.

6. DISCUSSION

Time lags between different spectral bands have been observed in accreting systems ranging from low-mass X-ray binaries to active galactic nuclei. A number of processes can produce these lags, such as the reprocessing of a source signal through inverse Compton scattering (Sunyaev & Titarchuk 1980; Payne 1980; Liang & Nolan 1984), reflection from an accretion disk or companion star (Basko et al. 1974; George & Fabian 1991), or disk wave propagation (Lyubarskii 1997; Kotov et al. 2001; Arévalo & Uttley 2006). We also refer the reader to Poutanen

(2001) for a review. Recently, sophisticated methods have been developed to relate spectral and timing variability using time lags to identify underlying processes or constrain the geometry of the emission (Casella et al. 2004; Reig et al. 2006; Uttley et al. 2011; Cassatella et al. 2012; Barret 2013). Many other accreting X-ray pulsars show time lags in their pulsed emission (e.g., Cui et al. 1998; Ibragimov et al. 2011; Falanga et al. 2012), but they appear quite different from what we observe in GS 0834−430. The phase lags seen in other accreting pulsars are usually seen in the soft band ($E < 5$ keV) and are of much lower magnitude (<0.05 cycles in phase). In this section, we discuss the possible origins of the large phase shifts (up to 80 keV) seen by *NuSTAR*.

Reflection from the accretion disk. Reflection of an X-ray signal off an accretion disk produces a very specific hardening of the spectrum (Basko et al. 1974; George & Fabian 1991). Lags are produced by the different path lengths and therefore the light travel times of the original and the reflected signals. The far edges of an accretion disk of radius R are expected to be geometrically thick, with the scale height H reaching up to $H/R \sim 0.5$ (White & Holt 1982). Therefore, the reflecting region can be quite far from the central source. In a binary, the X-ray emission can also be reflected off a dense stellar wind or the companion star. The energy dependency of the lags could possibly arise from the combined effect of the drop in the source signal and the rise of the reflected signal at different phases of the pulse.

However, we find this mechanism to be an unlikely explanation for the lags seen in GS 0834−430. First of all, a reflection model requires fine tuning to produce the smooth phase shift seen in Figure 3. In order to obtain a sharp reflected pulse, there would have to be only a narrow region of the accretion disk intersected by the pulsar beam, otherwise the reflected pulse would be spread by an amount proportional to the size of illuminated region. We note, however, that a geometry involving a warped disk might decrease the spread of the pulse (see, e.g., Hickox & Vrtilek 2005). The large orbit of this system ($a_x \sin i \sim 130$ lt-s; see Table 1) also rules out reflection from the surface of the companion star (see, e.g., Chester 1979), due to inconsistent timescales.

As a final remark, the very high reflected fraction that would be necessary to explain the hardening of the spectrum observed between intervals 7–9 in Figures 2 and 6 (we use the XSPEC model `reflect` to estimate that a covering fraction of ∼0.7 would be required) is inconsistent with the very low equivalent width of the iron line (George & Fabian 1991). The evolution of these phase-resolved spectra is instead well described by models commonly used to fit HMXB spectra. In such systems, the hard emission arises from soft photons being Compton upscattered in the accretion stream (Becker & Wolff 2007).

Comptonization by a corona. Inverse Compton scattering of soft X-rays off a hot electron corona that surrounds the compact object and the disk is an alternative way to produce hard lags and this process has been proposed as an explanation in some black hole binaries (e.g., Liang & Nolan 1984; Miyamoto et al. 1988; Dove et al. 1998; Lee & Miller 1998; Reig et al. 2000). The scattering that hardens the spectrum also introduces a delay in the reprocessed emission. If one assumes that the temperature of the corona is constant, that each scattering produces the same energy transfer, and that the flight time of the photons δ is the same between every scatter and is equal to the mean length between scatters in light seconds r/c, then it is easy to show that the total delay Δ introduced by the process is (Nowak et al. 1999)

$$\Delta \simeq n\delta \simeq \frac{r}{c}\frac{mc^2}{4kT_e}\ln\frac{E_n}{E_0}, \quad (4)$$

where n is the number of scatters to go from energy E_0 to E_n, mc^2 is the electron rest mass, and kT_e is the temperature of the electrons. By fitting the data in Figure 4 with the formula in Equation (4) and assuming an electron temperature of 50 keV, as is often observed in accreting sources, we obtain a mean flight length of $r/c \sim 0.5$ s, which is not unlikely in itself given that a large shocked region is expected around the neutron star in HMXBs, where the electron temperature can reach very high values (Nagae et al. 2004; Mauche et al. 2007).

This process has the advantage of smoothly relating the magnitude of the lag to the energy of the reprocessed photons. The main problem in this scenario is that Comptonized photons lose directional information after the first scatter. This fact means that to zeroth order, we would expect reprocessed photons coming from the different phases of the pulsar rotation to reach the observer at the same moment. Some work on a similar model has been done in the past for Her X-1 (Kuster et al. 2005), with the result that no sharp information can survive assuming this process.

This scenario is therefore unsuitable for explaining the very sharp shape of the lagged pulses, unless the Comptonizing region is not distributed uniformly around the source but is instead concentrated in a small region along the line of sight and is thus only illuminated in a well-determined pulse phase.

Pulsar beam shape-induced delays. In the accretion column of accreting X-ray pulsars, the combined effect of ram pressure from the infalling matter, radiation, the magnetic field, and gravitational effects can give rise to a complex beam structure with evolving spectral states driven mainly by the accretion rate (e.g., Blum & Kraus 2000; Leahy 2004a, 2004b; Becker et al. 2012). This complex structure is likely to show different spectra in different regions of the beam, as often seen in phase-resolved spectroscopy.

Accreting X-ray pulsars often show phase/time delays in their pulsed emission. There is a wide range of examples that appear phenomenologically different, suggesting that a single model does not apply to all sources. Soft lags, as opposed to the hard lags reported here, are quite common in accreting millisecond pulsars, such as SAXJ1808.4−3658 (Cui et al. 1998), IGR J17511−3057 (Ibragimov et al. 2011), or IGR J17498−2921 (Falanga et al. 2012), but their magnitude is below the ∼ms level. These lags can be modeled as a relativistic Doppler effect (the beam appears harder when it is moving toward the observer) or Compton down scattering in the accretion column. A similar behavior has been observed in burst oscillations (Ford 1999; Artigue et al. 2013). More peculiar behavior has been observed in the Be/X-ray binary 4U 0115+63 (Ferrigno et al. 2011), with unusual "waves" in the pulse phase lags that the authors convincingly attribute to an effect of cyclotron resonant scattering.

If the source has a luminosity around $\sim 10^{37}$ erg s^{-1}, as is the case for GS 0834−430 in outburst, the latest calculations show that a Compton shock forms in the accretion column but that the luminosity is not sufficient to produce a radiation dominated shock, which would completely decelerate the infalling material high above the neutron star surface (Becker et al. 2012). In this intermediate regime, a complex beam profile is present, with radiation emerging through the walls of the accretion

column (fan beam), as well as along the magnetic field lines (pencil beam), after being upscattered to high energies by inverse Compton scattering inside the accretion column. The fan and pencil beam components could in principle have different spectral properties and, given the right geometry, could create the phase-shift effect seen in the *NuSTAR* data through a gradual mixing of a softer and harder continuum.

The situation is even more complex as relativistic light bending can change the observed spectrum with pulse phase quite drastically, depending on the altitude above the neutron star (Kraus 2001). Furthermore, a filled accretion funnel is only the simplest geometry; strong evidence exists that the accretion column might be hollow for certain sources, with different spectra emerging from the inner and outer walls (A 0535+26, Caballero et al. 2011; Cen X−3, Kraus et al. 2003). These complex geometries could lead to the observed pulse profile shift in GS 0834−430.

Pulsar beams are known to be complex and diverse, while Comptonization and reflection are ubiquitous phenomena and corona and disk geometries are likely similar in different sources. We would therefore expect hard lags to appear in more systems were they caused by the latter effects.

7. CONCLUSIONS

We have analyzed observations of the accreting X-ray pulsar GS 0834−430 using the *NuSTAR* high-energy X-ray telescope. The spectrum of GS 0834−430 appears to be characteristic of those observed in HMXBs and is well described by the phenomenological models NPEX and FDCUT with parameter values within the ranges typically used to describe HMXB spectra. We detect a weak iron line (EW $\sim$ 40 eV), which appears mildly anticorrelated with the 5–10 keV flux. We find no evidence for a CRSF in either the phase-averaged or the phase-resolved spectra.

The pulse profile evolves strongly with energy. The 3–10 keV profile has two peaks, a secondary peak at phase 0.2 (relative to an arbitrary reference time) and a primary peak at phase 0.8.

We observe a strong phase shift of these peaks with energy, up to almost 0.3 in phase (about 4 s in time). The shift is almost linear at low energies, saturating above $\sim$40 keV. A significant phase shift of this magnitude at hard X-ray energies has not been observed before in an accreting X-ray pulsar. This shift is hard to explain as a result either of time lags due to reflection or Comptonization. The unusual spectral evolution with phase might be instead related to the detailed structure in the pulsar beam. In this case, our results will help shed light on the nature of the physical effects taking place in the pulsar accretion column.

This work was supported under NASA contract No. NNG08FD60C and made use of data from the *NuSTAR* mission, a project led by the California Institute of Technology, managed by the Jet Propulsion Laboratory, and funded by the National Aeronautics and Space Administration. We thank the *NuSTAR* Operations, Software, and Calibration teams for support with the execution and analysis of these observations. This research has made use of the *NuSTAR* Data Analysis Software (NuSTARDAS) jointly developed by the ASI Science Data Center (ASDC, Italy) and the California Institute of Technology (USA). Matteo Bachetti wishes to acknowledge the support from the Centre National d'Etudes Spatiales (CNES). Lorenzo Natalucci acknowledges financial support through contract ASI/INAF I/037/12/0.

REFERENCES

Aoki, T., Dotani, T., Ebisawa, K., et al. 1992, PASJ, 44, 641
Arévalo, P., & Uttley, P. 2006, MNRAS, 367, 801
Arnaud, K. A. 1996, ADASS, 101, 17
Artigue, R., Barret, D., Lamb, F. K., Lo, K. H., & Miller, M. C. 2013, MNRAS, 433, L64
Barret, D. 2013, ApJ, 770, 9
Barthelmy, S. D., Cummings, J. R., D'Avanzo, P., et al. 2012, GCN, 13388, 1
Basko, M. M., Sunyaev, R. A., & Titarchuk, L. G. 1974, A&A, 31, 249
Becker, P. A., Klochkov, D., Schönherr, G., et al. 2012, A&A, 544, 123
Becker, P. A., & Wolff, M. T. 2007, ApJ, 654, 435
Belloni, T., Hasinger, G., Pietsch, W., et al. 1993, A&A, 271, 487
Blum, S., & Kraus, U. 2000, ApJ, 529, 968
Buccheri, R., Bennett, K., Bignami, G. F., et al. 1983, A&A, 128, 245
Burrows, D. N., Hill, J. E., Nousek, J. A., et al. 2005, SSRv, 120, 165
Caballero, I., Kraus, U., Santangelo, A., Sasaki, M., & Kretschmar, P. 2011, A&A, 526, 131
Caballero, I., & Wilms, J. 2012, MmSAI, 83, 230
Casella, P., Belloni, T., Homan, J., & Stella, L. 2004, A&A, 426, 587
Cassatella, P., Uttley, P., Wilms, J., & Poutanen, J. 2012, MNRAS, 422, 2407
Chester, T. J. 1979, ApJ, 229, 1085
Coburn, W., Heindl, W. A., Rothschild, R. E., et al. 2002, ApJ, 580, 394
Coburn, W., Kretschmar, P., Kreykenbohm, I., et al. 2006, AdSpR, 38, 2747
Cui, W., Morgan, E. H., & Titarchuk, L. G. 1998, ApJL, 504, L27
Davidson, K., & Ostriker, J. P. 1973, ApJ, 179, 585
Dove, J. B., Wilms, J., Nowak, M. A., Vaughan, B. A., & Begelman, M. C. 1998, MNRAS, 298, 729
Drave, S. P., Sguera, V., Bird, A. J., et al. 2012, ATel, 4218, 1
Falanga, M., Kuiper, L., Poutanen, J., et al. 2012, A&A, 545, 26
Ferrigno, C., Falanga, M., Bozzo, E., et al. 2011, A&A, 532, 76
Ford, E. C. 1999, ApJL, 519, L73
Fürst, F., Pottschmidt, K., Kreykenbohm, I., et al. 2012, A&A, 547, A2
George, I. M., & Fabian, A. C. 1991, MNRAS, 249, 352
Harrison, F. A., Craig, W. W., Christensen, F. E., et al. 2013, ApJ, 770, 103
Hickox, R. C., & Vrtilek, S. D. 2005, ApJ, 633, 1064
Ibragimov, A., Kajava, J. J. E., & Poutanen, J. 2011, MNRAS, 415, 1864
Israel, G. L., Covino, S., Campana, S., et al. 2000, MNRAS, 314, 87
Jenke, P., Finger, M. H., & Connaughton, V. 2012, ATel, 4235, 1
Kalberla, P. M. W., Burton, W. B., Hartmann, D., et al. 2005, A&A, 440, 775
Kotov, O., Churazov, E., & Gilfanov, M. 2001, MNRAS, 327, 799
Kraus, U. 2001, ApJ, 563, 289
Kraus, U., Zahn, C., Weth, C., & Ruder, H. 2003, ApJ, 590, 424
Kuster, M., Wilms, J., Staubert, R., et al. 2005, A&A, 443, 753
Leahy, D. A. 2004a, MNRAS, 348, 932
Leahy, D. A. 2004b, ApJ, 613, 517
Leahy, D. A., Darbro, W., Elsner, R. F., et al. 1983, ApJ, 266, 160
Lee, H. C., & Miller, G. S. 1998, MNRAS, 299, 479
Liang, E. P., & Nolan, P. L. 1984, SSRv, 38, 353
Lyubarskii, Y. E. 1997, MNRAS, 292, 679
Makishima, K., Mihara, T., Nagase, F., & Tanaka, Y. 1999, ApJ, 525, 978
Mauche, C. W., Liedahl, D. A., Akiyama, S., & Plewa, T. 2007, PThPS, 169, 196
Meegan, C., Lichti, G., Bhat, P. N., et al. 2009, ApJ, 702, 791
Mihara, T. 1995, PhD thesis, University of Tokyo
Miyamoto, S., Kitamoto, S., Mitsuda, K., & Dotani, T. 1988, Natur, 336, 450
Müller, S., Ferrigno, C., Kühnel, M., et al. 2013, A&A, 551, 6
Nagae, T., Oka, K., Matsuda, T., et al. 2004, A&A, 419, 335
Nowak, M. A., Vaughan, B. A., Wilms, J., Dove, J. B., & Begelman, M. C. 1999, ApJ, 510, 874
Payne, D. G. 1980, ApJ, 237, 951
Poutanen, J. 2001, AdSpR, 28, 267
Reig, P., Belloni, T., van der Klis, M., et al. 2000, ApJ, 541, 883
Reig, P., Martínez-Núñez, S., & Reglero, V. 2006, A&A, 449, 703
Reig, P., & Nespoli, E. 2013, A&A, 551, 1
Schönherr, G., Wilms, J., Kretschmar, P., et al. 2007, A&A, 472, 353
Sunyaev, R. 1990, IAUC, 5122, 2
Sunyaev, R. 1991, IAUC, 5180, 1
Sunyaev, R. A., & Titarchuk, L. G. 1980, A&A, 86, 121
Tanaka, Y. 1986, in IAU Colloq. 89: Radiation Hydrodynamics in Stars and Compact Objects, ed. D. Mihalas & K.-H. A. Winkler (Lecture Notes in Physics, Vol. 255; Berlin: Springer), 198
Uttley, P., Wilkinson, T., Cassatella, P., et al. 2011, MNRAS, 414, L60
White, N. E., & Holt, S. S. 1982, ApJ, 257, 318
Wilms, J., Allen, A., & McCray, R. 2000, ApJ, 542, 914
Wilson, C. A., Finger, M. H., Harmon, B. A., et al. 1997, ApJ, 479, 388
Winkler, C., Courvoisier, T. J.-L., Di Cocco, G., et al. 2003, A&A, 411, L1